Check for updates

Highly selective conversion of CO_2 to methanol on the CuZnO–ZrO$_2$ solid solution with the assistance of plasma

Fennv Han, [ID] [a] Huaiping Liu,[b] Wenqiang Cheng[a] and Qi Xu*[ac]

CuZnO–ZrO$_2$–C was prepared by a co-precipitation method. For comparison, CuZnO–ZrO$_2$–PC and CuZnO–ZrO$_2$–CP were prepared by glow discharge plasma. The catalysts were characterized via the XRD, N$_2$ adsorption–desorption, TEM, SEM, EDS, XPS, CO_2-TPD and H$_2$-TPR techniques. The catalysts were comparatively investigated for CO_2 conversion and methanol selectivity in a fixed-bed reactor under the condition of 2 MPa, 250 °C, H$_2$/CO_2 = 3/1 and GHSV = 12 000 mL g^{-1} h^{-1}. The results showed that the activities of the catalysts increased in the order of CuZnO–ZrO$_2$–PC > CuZnO–ZrO$_2$–CP > CuZnO–ZrO$_2$–C. Moreover, the CO_2 conversion of CuZnO–ZrO$_2$–C increased by 38.9% via treatment with glow discharge plasma. The results are well explained based on the CO_2-TPD and H$_2$-TPR characterizations of the catalysts.

1. Introduction

The excessive consumption of fossil fuels leads to the increase in atmospheric CO_2 concentration. CO_2 is one of the main greenhouse gases, which causes the global temperature to rise more seriously. Therefore, conversion of CO_2 into value-added chemicals has attracted extensive attention of the researchers.[1–4] As an excellent C1 resource, CO_2 is often used to prepare high value-added chemicals, such as methane, methanol, formic acid, and so on.

Methanol from CO_2 hydrogenation is one of the most important means of utilization of CO_2 resource. Methanol is an important raw material for the synthesis of organic chemicals and can be used to synthesize formaldehyde and other chemical products.[5–7] Methanol is also a type of clean fuel, which can be blended into or substituted for gasoline as automobile fuels. Actually, the use of methanol has already been established for different applications such as in cars and fuel cells. In the 1960s, commercial Cu/ZnO/Al$_2$O$_3$ catalysts were used in the production of industrial methanol at operating temperatures of 240–260 °C and reaction pressures of 5–10 MPa. However, at present, the selectivity of copper-based catalysts towards the methanol production from CO_2 hydrogenation is low. Therefore, it is urgent to either improve copper-based catalysts or develop new catalysts. Consequently, the research on the process route of methanol production from CO_2 hydrogenation is focused on the catalysts. Some studies have shown that conversion of CO_2 to methanol reaction is a structure-sensitive reaction. Besides, different preparation methods of catalysts lead to different structures of catalysts, thus affecting the activity of catalysts.[8,9] The Cu/ZnO catalytic system is the basic copper-based catalyst, wherein zinc oxide can improve the dispersion and stability of copper, and lattice oxygen vacancies and paired electrons in zinc oxide can promote the methanol synthesis. Other catalysts, such as Cu/ZnO/SiO$_2$, Cu/ZnO/ZrO$_2$, Cu/ZnO/Al$_2$O$_3$ and Cu/ZnO/TiO$_2$, are generally modified on this basis. ZrO$_2$ is considered as a good carrier of Cu/ZnO as it provides active sites for CO and CO_2 for the insertion into Zr–OH, and Cu provides active hydrogen for ZrO$_2$ to hydrogenate formate and hydroxycarbonate to methanol on the ZrO$_2$ surface. Simultaneously, the addition of ZrO$_2$ can also improve the dispersion of active component copper. Moreover, ZrO$_2$ has low hydrophilicity, which can promote the catalytic activity.

Low temperature plasma is also widely used in the field of catalysis, including for catalysts used to synthesize ultrafine particles, surface treatment of catalysts and regeneration of catalysts. Catalysts prepared by a low temperature plasma-assisted synthesis generally have the advantages such as high dispersion, small catalyst particle size, large specific surface area and lattice defects. Bagherzadeh[10] et al. prepared CuO/ZnO/Al$_2$O$_3$ nanocatalysts by a hydrothermal synthesis and coprecipitation method, and then exposed to glow discharge plasma for 45 min at 1000 V. The results showed that the methanol conversion of CuO/ZnO/Al$_2$O$_3$ catalysts synthesized by plasma-assisted coprecipitation was the highest. Seyedi[11] et al. synthesised a series of CuO–ZnO–Al$_2$O$_3$–ZrO$_2$

aSchool of Chemistry and Chemical Engineering, Yancheng Institute of Technology, Yancheng 224051, PR China. E-mail: ycxqsteve@163.com; Fax: +86-515-88298655; Tel: +86-515-88298655

bKunYue Interconnection Environmental Technology (JiangSu) Co., LTD, Yancheng 224051, PR China

cKey Laboratory under Construction for Volatile Organic Compounds Controlling of Jiangsu Province, Yancheng 224051, PR China

nanocatalysts *via* hydrothermal, thermo-chemical and coprecipitation-plasma methods. The results showed that the catalysts treated by argon glow discharge plasma had a smaller particle size, better dispersibility and larger specific surface area, which could improve the hydrogen yield and methanol conversion.

In this study, $CuZnO–ZrO_2$ catalysts were prepared *via* the plasma-assisted coprecipitation method. The catalysts were characterized and analyzed *via* the XRD, Nitrogen physical adsorption, TEM, XPS and H_2-TPR techniques. The methanol synthesis performance of the catalysts before and after the glow discharge plasma modification was studied. The effects of the reaction temperature and stability of the catalyst were also investigated.

2. Experimental section

2.1 Preparation of catalysts

A mixed solution of metal nitrate was prepared by completely dissolving $Zn(NO_3)_2 \cdot 6H_2O$, $Zr(NO_3)_4 \cdot 5H_2O$ and $Cu(NO_3)_2 \cdot 3H_2O$ (Cu/Zn/Zr = 1/4/15) in deionized water. The solution with metal nitrates and 0.5 mol L^{-1} Na_2CO_3 solution were added into a reaction vessel at 70 °C. The final pH of titration was about 7.5. After the titration, the solution was stirred at 70 °C for 1 h, followed by ageing for 3 h. After cooling to room temperature, the solution was centrifuged and the precipitate was washed three times with deionized water to remove Na^+ ions. The precipitate was dried in a vacuum drying chamber for 12 h to obtain the catalyst precursor.

The sample was then calcined in muffle furnace at 500 °C for 3 h and was denoted as $CuZnO–ZrO_2$–C. This sample of the catalyst precursor was treated with a glow discharge plasma equipment for 15 min and roasted for 3 h in a muffle furnace at 500 °C and was denoted as $CuZnO–ZrO_2$–PC. Similarly, the sample of the catalyst precursor calcined in the muffle furnace at 500 °C for 3 h and then treated by plasma for 15 min and was denoted as $CuZnO–ZrO_2$–CP.

2.2 Characterization techniques

The XRD patterns of the catalysts were obtained at room temperature on a PANalytical X'Pert Pro X-ray diffractometer at 40 kV and 40 mA over 20° to 80° 2θ range with Cu Kα radiation (λ = 0.15416 nm). N_2 adsorption–desorption isotherms for the catalysts were recorded on a Beckman coulter SA 3100 type specific surface area and aperture measurement instrument at −196 °C. The size distribution of micropores was determined using the Horvarth–Kawazoe(H–K) equation. The surface areas of the catalysts were calculated by the Brunauer–Emmett–Teller (BET) method. Transmission Electron Microscopy (TEM) images were recorded on a JEOL JEM-2100F TEM instrument at an accelerating voltage of 200 kV. The morphology of the catalyst was analyzed *via* scanning electron microscopy (SEM 450, Nova nano, Japan). The elemental chemical states of the samples were analyzed *via* X-ray photoelectron spectroscopy (XPS) using a Thermo Scientific Escalab 250Xi X-ray spectrometer with binding energy corrected by C 1s (284.8 eV). The

basicity of the catalyst was measured by temperature-programmed desorption of CO_2 (CO_2-TPD) techniques on an AutoChem II 2910 instrument (Micromeritics, USA). The reduction behavior of the catalysts was studied *via* hydrogen programmed temperature-reduction (H_2-TPR) using a Micromeritics AutoChemII 2920 instrument equipped with a thermal conductivity detector (TCD).

2.3 Photocatalytic conversion of CO_2

The photocatalytic conversion of CO_2 to methanol was performed in an HP-WF51 fixed bed reactor (the inner diameter of a stainless steel reaction tube was 10 mm). Typically, 0.5 g of each catalyst (40–80 mesh) diluted with 0.5 g quartz sands was pre-treated at a pressure of 0.2 MPa in a flow of 50% H_2/N_2 stream (20 mL min^{-1}) at 280 °C for 4 h. Then, syngas ($V(H_2) : V(CO_2) : V(N_2) = 72 : 24 : 4$) was applied, and the reaction was began with the desired reaction parameters.

CO_2, N_2 and CO were analyzed *via* gas chromatography (6820, Agilent) with a thermal conductivity detector (TCD) equipped with a TDX-01 carbon molecular sieve column. Methanol and other hydrocarbons were analyzed using a flame ionization detector (FID) equipped with a Porapak Q column.

Conversion of CO_2, product selectivity and yield of methanol were calculated by the following eqn (1)–(4).

$$X(\mathrm{CO_2}) = (f_{\mathrm{CO}}A_{\mathrm{CO}} + f_{\mathrm{CH_3OH}}A_{\mathrm{CH_3OH}})/(f_{\mathrm{CO}}A_{\mathrm{CO}} + f_{\mathrm{CH_3OH}}A_{\mathrm{CH_3OH}} + f_{\mathrm{CO_2}}A_{\mathrm{CO_2}}) \tag{1}$$

$$S(\mathrm{CH_3OH}) = (f_{\mathrm{CH_3OH}}A_{\mathrm{CH_3OH}})/(f_{\mathrm{CH_3OH}}A_{\mathrm{CH_3OH}} + f_{\mathrm{CO}}A_{\mathrm{CO}}) \tag{2}$$

$$S(\mathrm{CO}) = f_{\mathrm{CO}}A_{\mathrm{CO}}/(f_{\mathrm{CO}}A_{\mathrm{CO}} + f_{\mathrm{CH_3OH}}A_{\mathrm{CH_3OH}}) \tag{3}$$

$$Y(\mathrm{CH_3OH}) = X(\mathrm{CO_2}) \times S(\mathrm{CH_3OH}) \tag{4}$$

A_i represents the peak area of various products in the GC analysis and f_i represents their correction factors.

3. Results and discussion

3.1 Catalyst characterization

3.1.1 XRD analysis. XRD was used to analyze the crystalline structure of the catalysts, and the XRD patterns of $CuZnO–ZrO_2$–C, $CuZnO–ZrO_2$–PC and $CuZnO–ZrO_2$–CP catalysts are shown in Fig. 1. It could be seen that the catalysts exhibited four characteristic diffraction peaks at 2θ = 30.5°, 35.2°, 50.9°, and 60.3° correspond to the (011), (110), (112) and (121) planes of tetragonal phase t-ZrO_2.[12,13] In addition, the typical diffraction peaks of monoclinic CuO are observed only in the $CuZnO–ZrO_2$–C catalyst, which indicated that copper species in the $CuZnO–ZrO_2$–C catalyst was CuO.[14,15] No obvious diffraction peaks of zinc oxide can be found, as shown in the Fig. 1. Due to sufficient crystallization of ZrO_2 during calcination, Zn^{2+} ions might have entered the lattice of zirconia and stabilized tetragonal zirconia. As shown, the diffraction peaks of CuO disappeared after the plasma treatment ($CuZnO–ZrO_2$–PC and $CuZnO–ZrO_2$–CP). It might be that CuO lost its crystallinity and became amorphous, and highly dispersed after the plasma treatment. Three forms of
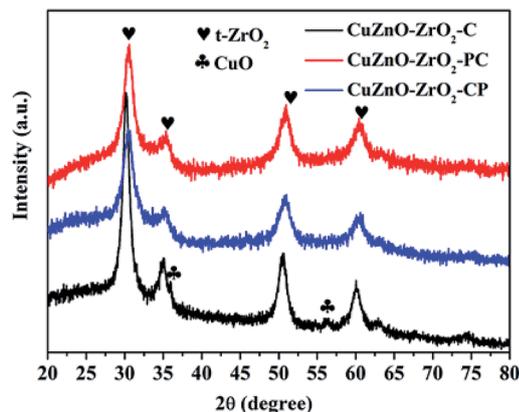
Fig. 1 XRD patterns of catalyst before and after modification by plasma.

Table 1 Summary of the N_2 physisorption data of catalysts

	Specific surface area (m^2 g^{-1})	Pore volume (cm^3 g^{-1})	Mean pore size (nm)
CuZnO–ZrO$_2$–C	24.48	0.055	9.05
CuZnO–ZrO$_2$–PC	24.57	0.035	5.98
CuZnO–ZrO$_2$–CP	25.38	0.056	8.90

copper species were observed in solid solution: lattice doped, surface dispersed and bulk. The highly dispersive CuO on the catalyst surface is considered to be the most active form compared to the bulk CuO and lattice CuO. The intensity of the diffraction peaks of t-ZrO_2 decreased after the plasma treatment, indicating that the crystallinity of catalysts after the plasma treatment decreased compared with that of the catalyst directly roasted, and the catalyst modified by plasma had good dispersion.

3.1.2 N_2 adsorption–desorption analysis. The N_2 adsorption–desorption isotherms of the catalysts are shown in Fig. 2. Regardless of the treatment method used, each of the catalyst showed a type IV isotherm, together with an H3 hysteresis loop based on the IUPAC classification, which was characterized as a mesoporous structure.[16–18] The summary of N_2 physisorption data of catalysts are reported in Table 1. The specific surface area of CuZnO–ZrO$_2$–C, CuZnO–ZrO$_2$–PC and CuZnO–ZrO$_2$–CP catalysts as calculated by BET equation was 24.48 m^2 g^{-1}, 24.57 m^2 g^{-1} and 25.38 m^2 g^{-1}, respectively. The results also showed

that the specific surface area of the catalyst treated with plasma did not change. The pore size distributions (PSDs) determined by the BJH method based on the desorption branch are shown in Fig. 2. A peak centered at 4 nm was observed for CuZnO–ZrO$_2$–C. CuZnO–ZrO$_2$–CP showed the same peak maximum at about 4 nm. The peak maxima of the PSDs for CuZnO–ZrO$_2$–PC clearly shifted to smaller size, suggesting a higher homogeneous dispersion of metal oxides. According to the pore size distribution curve, the radius corresponding to the highest point was about 2–5 nm, which indicated that the pore diameter distribution of catalysts was mainly mesoporous.

3.1.3 Structural morphology analysis. To investigate the structural morphology of the catalysts, TEM and HRTEM images were recorded, as shown in Fig. 3. It can be seen that the CuZnO–ZrO$_2$–C catalyst had no obvious edge (Fig. 3A), and the agglomeration of catalyst particles was obvious. However, the particle distribution of the catalysts (CuZnO–ZrO$_2$–PC and CuZnO–ZrO$_2$–CP) treated by plasma was more uniform, and the agglomeration phenomenon was obviously improved, particularly in the case of plasma modification before calcination. The HRTEM images revealed that the lattice fringes with the d-spacing of 0.293 nm corresponded to the (011) lattice plane of t-ZrO_2. The SEM image of CuZnO–ZrO$_2$–PC was is shown in Fig. 4A. Each particle arranged tightly to form a granular layer and Zn^{2+} ions completely entered the lattice of zirconia. It can be seen that CuO might exist in the amorphous form and is highly dispersed, which was consistent with the results of XRD.
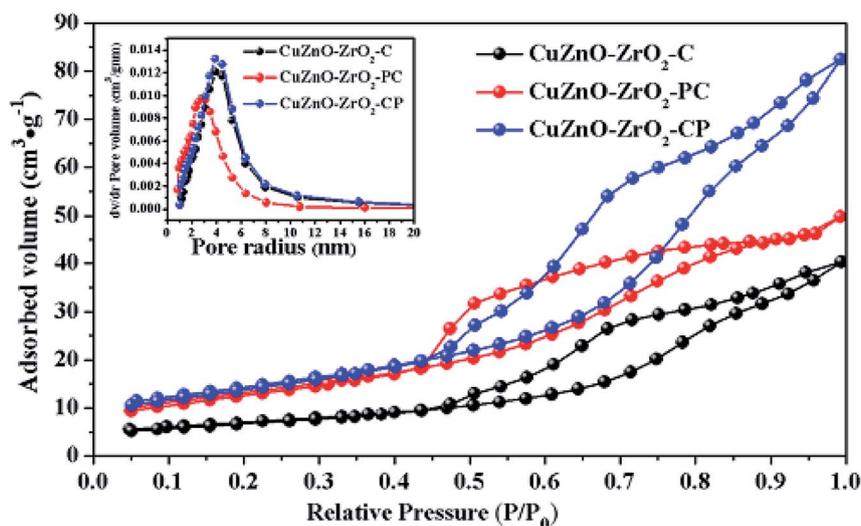

Fig. 2 N_2 adsorption–desorption and pore diameter distribution isotherms of the catalysts.

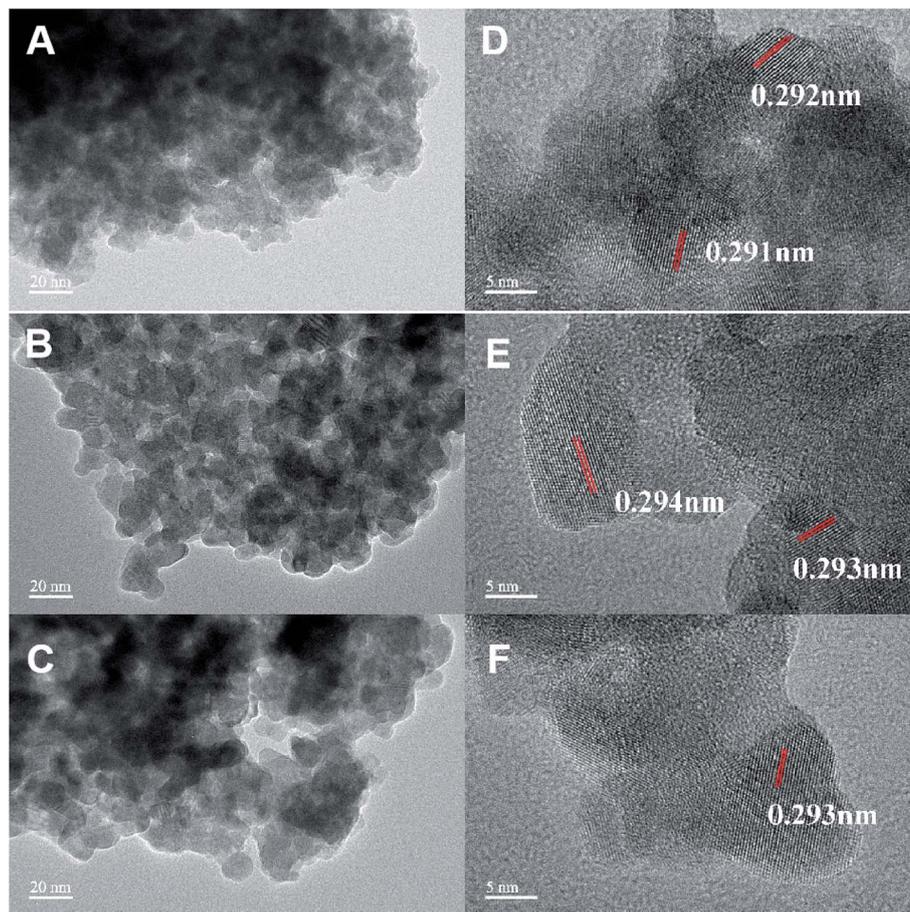Fig. 3 TEM images (A) of CuZnO–ZrO$_2$–C, (B) of CuZnO–ZrO$_2$–PC, (C) of CuZnO–ZrO$_2$–CP. HRTEM images (D) of CuZnO–ZrO$_2$–C, (E) of CuZnO–ZrO$_2$–PC, (F) of CuZnO–ZrO$_2$–CP.

Fig. 4B showed that the distribution of the Cu, Zn, Zr, and O elements was uniform throughout the sample.

3.1.4 XPS analysis. To further investigate the electronic structures and chemical environment of Zn, Zr, Cu, O, XPS spectra were recorded, as shown in Fig. 5. Fig. 5A revealed a wide-range XPS spectra of CuZnO–ZrO$_2$–C, CuZnO–ZrO$_2$–PC

and CuZnO–ZrO$_2$–CP catalysts. It was clear that catalysts exhibited Zn, Zr, Cu, O, C and Na elements. Amongst them, C 1s was the external pollution peak, which might have been due to the hydrocarbon present in the conductive adhesive on the instrument used during XPS analysis. The Na 1s peak appeared becuase of Na$_2$CO$_3$ solution as precipitating agent during
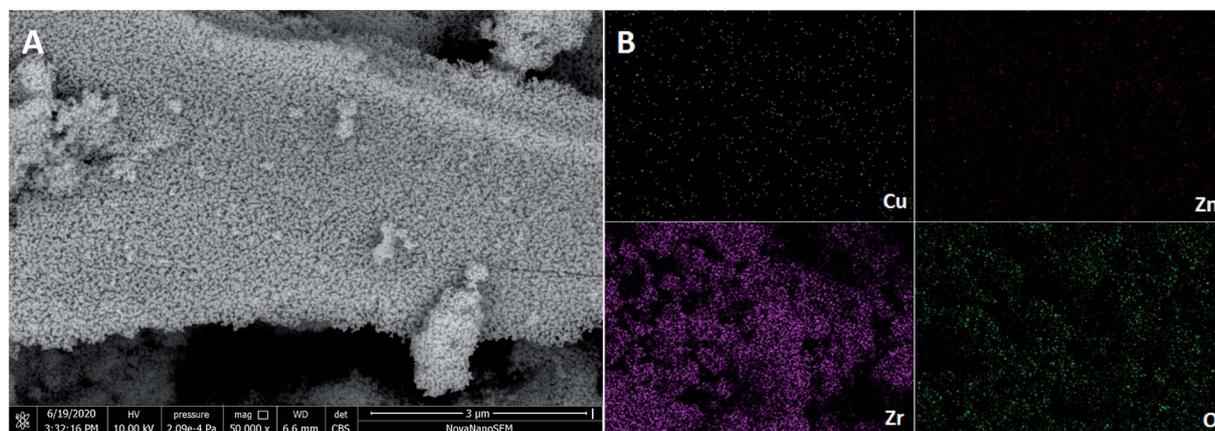

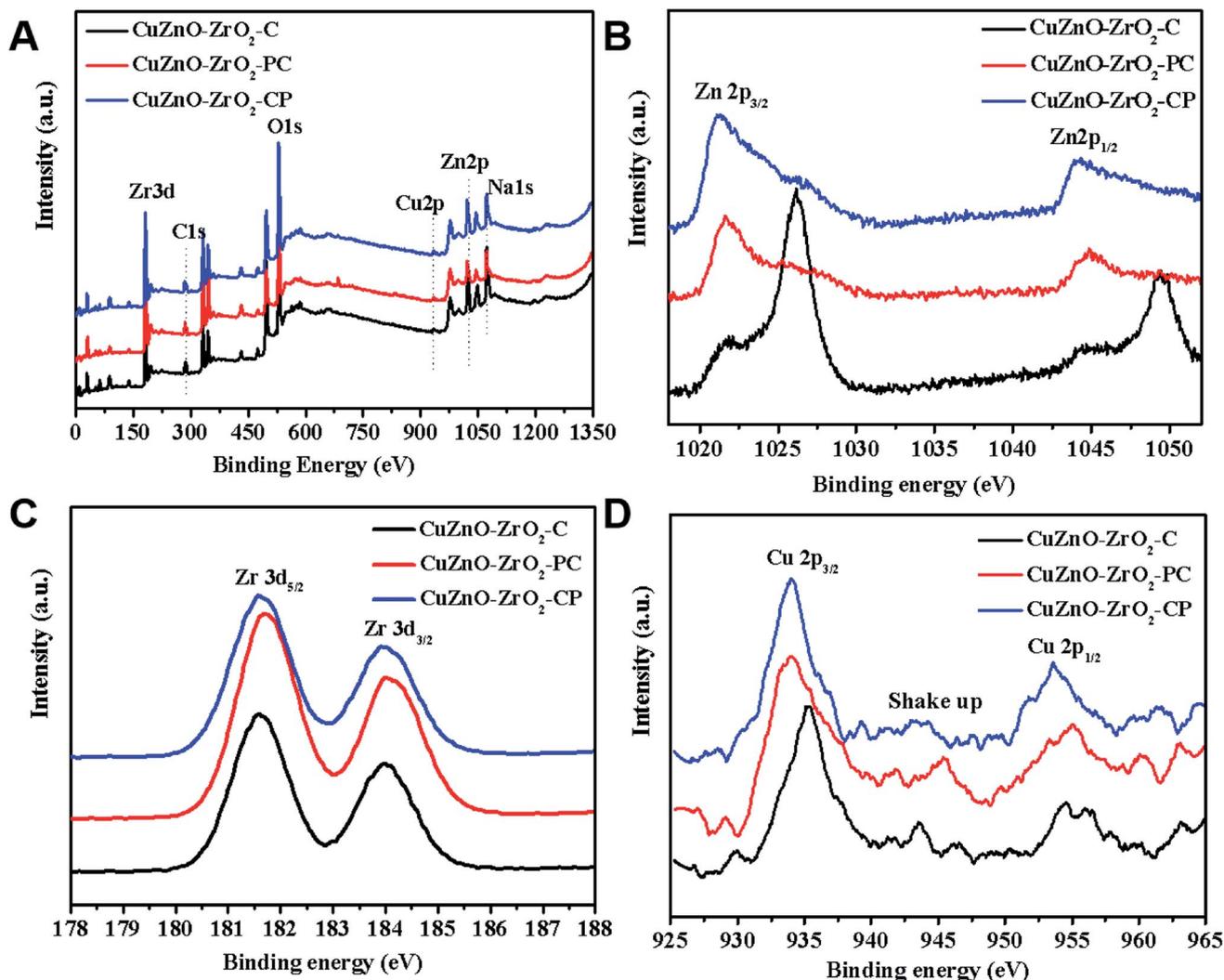Fig. 4 SEM images of CuZnO–ZrO$_2$–PC (A) and distribution diagram of Cu, Zn, Zr, O elements (B).

Fig. 5 XPS survey spectra (A), high resolution XPS spectra of Zn 2p (B), high resolution XPS spectra of Zr 3d (C), high resolution XPS spectra of Cu 2p (D).

preparation of catalyst and the incomplete washing up of Na^+ during precipitation washing. The high resolution XPS spectra of Zn 2p (Fig. 5B) exhibited two peaks at binding energies of 1021 and 1044 eV, corresponding to Zn $2p_{3/2}$ and Zn $2p_{1/2}$, respectively, which proved that Zn element existed in the form of Zn^{2+} in the catalyst.[19] The binding energy of Zn 2p of the plasma-treated catalyst decreased by about 4.5 eV, which indicated that the density of the electron cloud around Zn 2p changed significantly and the chemical environment was altered after the plasma treatment of the catalyst. The high resolution XPS spectra of Zr 3d (Fig. 5C) revealed the presence of two peaks located at the binding energies of 182 and 184 eV, corresponding to Zr $3d_{5/2}$ and Zr $3d_{3/2}$, respectively. Compared with the untreated catalyst, the binding energy of Zr 3d basically did not change, indicating that the chemical environment and energy state around Zr 3d of the plasma-treated catalyst did not change.[19] XPS spectra of the high-resolution orbital of Cu 2p are shown in Fig. 5D, and the binding energy of catalysts at 935 and 954 eV correspond to the two characteristic peaks of Cu $2p_{3/2}$

and Cu $2p_{1/2}$, respectively. Simultaneously, strong satellite peaks appeared in 940–945 eV, which proved that the Cu element exists in the form of Cu^{2+} in the catalyst,[20] and the binding energy of Cu $2p_{3/2}$ of the plasma-treated catalyst sample decreased by about 1.2 eV, indicating that the energy state and chemical environment of the Cu species in the catalyst changed. The peak position of Zn 2p and Cu 2p moved to a lower binding energy level, which is responsible for improving the reduction capacity of the catalyst.[21]

3.1.5 CO₂-TPD analysis. Fig. 6 displays the CO₂-TPD profiles of the catalysts, the CO₂ desorption curve of CuZnO–ZrO₂–C and CuZnO–ZrO₂–CP catalysts showed two strong peaks. Peaks located at the low temperature are ascribed to weakly adsorbed carbon species at weakly basic sites. These weakly basic sites are related to the hydroxyl group (Zr–OH). Peaks located at the high temperature corresponded to the strongly basic sites, such as coordination oxygen atoms.[22] The CuZnO–ZrO₂–PC catalyst showed another peak at 294.3 °C, corresponding to the moderately basic sites, which is related to
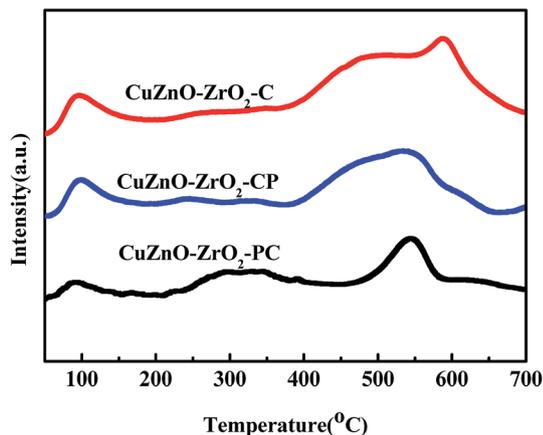
Fig. 6 CO_2-TPD patterns of catalysts.

the metal–oxygen pairs.[22] Considering that the reaction temperature was at 210–290 °C, moderately basic sites seemed to be more correlated to the active sites for CO_2 hydrogenation compared to the other basic sites. Therefore, it was speculated that CuZnO–ZrO2–PC would exhibit the best CO_2 conversion and CH_3OH selectivity, which was consistent with the results of catalytic performance.

3.1.6 H_2-TPR analysis. H_2-TPR could be used to analyze the reduction performance of metal oxide catalysts. The H_2-TPR profiles of the catalysts are shown in Fig. 7. The CuZnO–ZrO2–C catalyst showed a hydrogen consumption peak at 310.0 °C, which is attributed to the reduction of CuO species.[23] The reduction temperature of CuO on the CuZnO–ZrO2–PC and CuZnO–ZrO2–CP catalysts were both lower than that of the CuZnO–ZrO2–C catalyst, particularly the CuZnO–ZrO2–PC catalyst, which could be due to the strong interaction between metal oxides in the catalyst.[24] The results show that the plasma-modified catalyst enhanced the catalytic performance and improved the catalytic activity of the catalyst. Considering that the reduction temperature was 280 °C, CuO on the CuZnO–ZrO2–PC catalyst is speculated to completely reduce to Cu^0. Hence, CuZnO–ZrO2–PC would exhibit the best CO_2 conversion
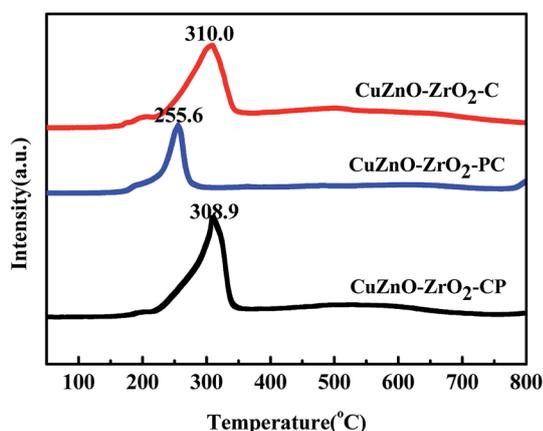

Fig. 7 H_2-TPR patterns of catalysts.

and CH_3OH selectivity, which was consistent with the results of catalytic performance.

3.2 Catalytic performance

3.2.1 Effect of plasma modification on catalytic performance. The performance of CuZnO–ZrO2–C, CuZnO–ZrO2–PC and CuZnO–ZrO2–CP catalysts at 2 MPa, 250 °C, H_2/CO_2 = 3/1 and GHSV = 12 000 mL g^{-1} h^{-1} are shown in Table 2. Compared with the CuZnO–ZrO2–C catalyst, the CO_2 conversion rate of the plasma-treated catalysts significantly increased; the CO_2 conversion of CuZnO–ZrO2–PC and CuZnO–ZrO2–CP catalysts increased by 39.8% and 33.9%, respectively, while methanol selectivity changes were not obvious. The results showed that the CO_2 conversion over the plasma-modified catalyst significantly increased, and the catalytic activity of the catalyst effectively improved, but the selectivity of methanol did not significantly improve.

3.2.2 Effect of the reaction temperature on catalytic performance. The effect of reaction temperature (the range of 210–290 °C) on catalytic performance is shown in Fig. 8. As shown in Fig. 8A, with the increase in the reaction temperature, the conversion of CO_2 increased, accompanied by a decrease in methanol selectivity, which was the result of a competition between the methanol synthesis and reverse water gas reaction. The methanol synthesis reaction is an exothermic reaction, while reverse water gas reaction is an endothermic reaction.[25] As shown in Fig. 8B, the methanol yield of all catalysts first increased with the increase in temperature; however, after reaching a certain value, the methanol yield decreased with the rise in temperature. At the maximum methanol yield of the CuZnO–ZrO2–C catalyst, the corresponding temperature was about 250 °C, while when the methanol yield of CuZnO–ZrO2–PC catalyst was the maximum, the corresponding temperature was about 270 °C, which indicated that the catalyst treated by plasma still had a higher catalytic activity at higher temperature values. This suggests that CuZnO–ZrO2–PC had a better high-temperature resistance. Obviously, the catalytic effect of CuZnO–ZrO2–PC and CuZnO–ZrO2–CP catalysts was better than that of the CuZnO–ZrO2–C catalyst.

3.2.3 Stability test of catalysts. In order to study the influence of plasma modification on the stability of the catalyst, the CuZnO–ZrO2–C and CuZnO–ZrO2–PC catalysts were tested in a fixed bed reactor under the following condition of P = 2 MPa, T = 250 °C, H_2/CO_2 = 3/1 and GHSV = 12 000 mL g^{-1} h^{-1}. As shown in Fig. 9, after the catalysts were used in a fixed bed

Table 2 Catalytic performance of CuZnO–ZrO2–C, CuZnO–ZrO2–PC and CuZnO–ZrO2–CP[a]

Catalysts	$X(CO_2)$/%	$S(CH_3OH)$/%	$S(CO)$/%	$Y(CH_3OH)$/%
CuZnO–ZrO2–C	10.3	74.1	25.9	7.6
CuZnO–ZrO2–PC	14.4	78.2	21.8	11.3
CuZnO–ZrO2–CP	13.8	74.2	25.8	10.2

[a] Condition: P = 2 MPa, T = 250 °C, H_2/CO_2 = 3/1 and GHSV = 12 000 mL g^{-1} h^{-1}.
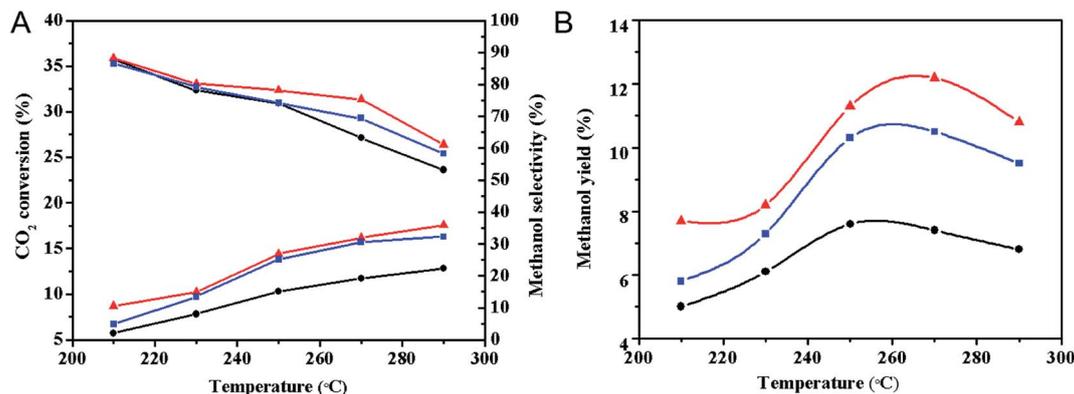
Fig. 8 Effect of reaction temperature on the (A) CO_2 conversion and (B) methanol selectivity over the different catalysts. (●) $CuZnO-ZrO_2-C$, (▲) $CuZnO-ZrO_2-PC$ and (■) $CuZnO-ZrO_2-CP$.
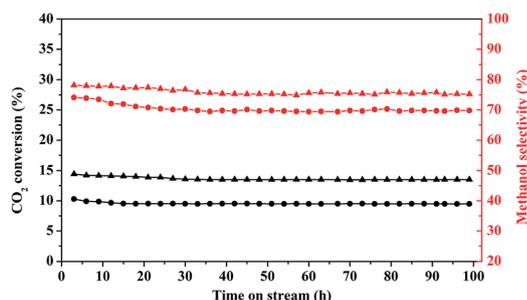

Fig. 9 The conversion of CO_2 and the selectivity of CH_3OH with reaction time over the catalysts. (●) $CuZnO-ZrO_2-C$ (▲) $CuZnO-ZrO_2-PC$.

reactor for a long time of 100 h, the CO_2 conversion of the $CuZnO-ZrO_2-C$ catalyst decreased by 7.8% (from 10.3% to 9.5%), and the methanol selectivity decreased by 5.8% (from 74.1% to 69.8%). However, the CO_2 conversion of the $CuZnO-ZrO_2-PC$ catalyst decreased by 6.3% (from 14.4% to 13.5%), and the methanol selectivity decreased by 3.8% (from 78.2% to 75.2%).

4. Conclusions

The $CuZnO-ZrO_2$ catalysts were pretreated by the glow discharge plasma before and after calcination. Compared with the $CuZnO-ZrO_2-C$ catalyst, the performance of the catalyst modified by plasma was better, the CO_2 conversion of $CuZnO-ZrO_2-PC$ increased by 39.8%, and the methanol yield increased by 48.7%. The XRD characterization showed that the plasma-modified catalyst had a lower crystallinity and a better dispersion, and the characterization of CO_2-TPD and H_2-TPR provided a basis for the better catalytic performance of plasma-modified catalysts.

Conflicts of interest

There are no conflicts to declare.

Acknowledgements

References

1 M. Kumar, S. Sundaram, E. Gnansounou, *et al.*, Carbon dioxide capture, storage and production of biofuel and biomaterials by bacteria: a review, *Bioresour. Technol.*, 2018, **247**, 1059–1068.

2 L. V. Alexander, X. Zhang, T. C. Peterson, *et al.*, Global observed changes in daily climate extremes of temperature and precipitation, *J. Geophys. Res.: Atmos.*, 2006, **111**(D5), 1042–1063.

3 P. Zhang, J. He, X. Hong, *et al.*, Carbon sources/sinks analysis of land use changes in China based on data envelopment analysis, *J. Cleaner Prod.*, 2018, **204**, 702–711.

4 K. Samson, M. Śliwa, R. P. Socha, *et al.*, Influence of ZrO_2 Structure and Copper Electronic State on Activity of Cu/ZrO_2 Catalysts in Methanol Synthesis from CO_2, *ACS Catal.*, 2016, **4**(10), 3730–3741.

5 K. Saravanan, H. Ham, N. Tsubaki, *et al.*, Recent progress for direct synthesis of dimethyl ether from syngas on the heterogeneous bifunctional hybrid catalysts, *Appl. Catal., B*, 2017, **217**, 494–522.

6 X. Zhou, T. Su, Y. Jiang, *et al.*, $CuO-Fe_2O_3-CeO_2$/HZSM-5 bifunctional catalyst Hydrogenated CO_2 for enhanced dimethyl ether synthesis, *Chem. Eng. Sci.*, 2016, **153**, 10–20.

7 C. A. Huff and M. S. Sanford, Cascade Catalysis for the Homogeneous Hydrogenation of CO_2 to Methanol, *J. Am. Chem. Soc.*, 2011, **133**(45), 18122–18125.

8 C. Liu, M. Li, J. Wang, *et al.*, Plasma methods for preparing green catalysts: current status and perspective, *Chin. J. Catal.*, 2016, **37**(3), 340–348.

9 J. Ye, C. Liu, D. Mei, *et al.*, Active oxygen vacancy site for methanol synthesis from CO_2 hydrogenation on In_2O_3 (110): a DFT study, *ACS Catal.*, 2013, **3**(6), 1296–1306.

10 S. B. Bagherzadeh and M. Haghighi, Plasma-enhanced comparative hydrothermal and coprecipitation preparation of $CuO/ZnO/Al_2O_3$ nanocatalyst used in hydrogen production *via* methanol steam reforming, *Energy Convers. Manage.*, 2017, **142**, 452–465.

11 A. M. Seyedi, M. Haghighi and N. Rahemi, Significant influence of cutting-edge plasma technology on catalytic properties and performance of $CuO–ZnO–Al_2O_3–ZrO_2$ nanocatalyst used in methanol steam reforming for fuel cell grade hydrogen production, *Ceram. Int.*, 2017, **43**(8), 6201–6213.

12 J. Wang, G. Li, Z. Li, *et al.*, A highly selective and stable $ZnO–ZrO_2$ solid solution catalyst for CO_2 hydrogenation to methanol, *Sci. Adv.*, 2017, **3**(10), e1701290.

13 K. Cheng, B. Gu, X. Liu, *et al.*, Direct and highly selective conversion of synthesis gas into lower olefins: design of a bifunctional catalyst combining methanol synthesis and carbon–carbon coupling, *Angew. Chem.*, 2016, **55**(15), 4725–4728.

14 W. Shan, W. Shen and C. Li, Structural Characteristics and Redox Behaviors of $Ce_{1-x}Cu_xO_y$ Solid Solutions, *Chem. Mater.*, 2003, **15**(25), 4761–4767.

15 W. T. Yao, S. H. Yu, Y. Zhou, *et al.*, Formation of uniform CuO nanorods by spontaneous aggregation: Selective synthesis of CuO, Cu_2O, and Cu nanoparticles by a solid–liquid phase arc discharge process, *J. Phys. Chem. B*, 2005, **109**(29), 14011–14016.

16 J. Y. LuO, M. Meng, X. Li, *et al.*, Mesoporous $Co_3O_4–CeO_2$ and $Pd/Co_3O_4–CeO_2$ catalysts: synthesis, characterization and mechanistic study of their catalytic properties for low-temperature CO oxidation, *J. Catal.*, 2008, **254**(2), 310–324.

17 Y. Yu, Y. M. Chan, Z. Bian, *et al.*, Enhanced performance and selectivity of CO_2 methanation over g-C_3N_4 assisted synthesis of $NiCeO_2$ catalyst: kinetics and DRIFTS studies, *Int. J. Hydrogen Energy*, 2018, **43**(32), 15191–15204.

18 Y. Yu, Z. Bian, F. Song, *et al.*, Influence of Calcination Temperature on Activity and Selectivity of $Ni–CeO_2$ and $Ni–Ce_{0.8}Zr_{0.2}O_2$ Catalysts for CO_2 Methanation, *Top. Catal.*, 2018, **61**(15–17), 1514–1527.

19 J. Xiao, D. Mao, X. Guo, *et al.*, Effect of TiO_2, ZrO_2, and TiO_2–ZrO_2 on the performance of $CuO–ZnO$ catalyst for CO_2 hydrogenation to methanol, *Appl. Surf. Sci.*, 2015, **338**, 146–153.

20 S. T. Hossain, E. Azeeva, K. Zhang, *et al.*, A comparative study of CO oxidation over Cu–O–Ce solid solutions and CuO/CeO_2 nanorods catalysts, *Appl. Surf. Sci.*, 2018, **455**, 132–143.

21 H. Zhu, R. Razzaq, C. Li, *et al.*, Catalytic Methanation of Carbon Dioxide by Active Oxygen Material $Ce_xZr_{1-x}O_2$ Supported Ni–Co Bimetallic Nanocatalysts, *AIChE J.*, 2013, **59**, 2567–2576.

22 T. Witoon, N. Kachaban, W. Donphai, *et al.*, Tuning of catalytic CO_2 hydrogenation by changing composition of $CuO–ZnO–ZrO_2$ catalysts, *Energy Convers. Manage.*, 2016, **118**, 21–31.

23 H. Lei, R. Nie, G. Wu and Z. Hou, Hydrogenation of CO_2 to CH_3OH over Cu/ZnO catalysts with different ZnO morphology, *Fuel*, 2015, **154**, 161–166.

24 G. Wang, D. Mao, X. Guo, *et al.*, Enhanced performance of the $CuO–ZnO–ZrO_2$ catalyst for CO_2 hydrogenation to methanol by WO_3 modification, *Appl. Surf. Sci.*, 2018, **456**, 403–409.

25 E. Moretti, L. Storaro, A. Talon, *et al.*, Effect of thermal treatments on the catalytic behaviour in the CO preferential oxidation of a $CuO–CeO_2–ZrO_2$ catalyst with a flower-like morphology, *Appl. Catal., B*, 2011, **102**(3–4), 627–637.